Available online at www.sciencedirect.com
ScienceDirect
Ceramics International 35 (2009) 2667–2674
CERAMICS INTERNATIONAL
www.elsevier.com/locate/ceramint

Thermodynamics of densification of powder compact

Yoshihiro Hirata [a,*], Akihiro Hara [a], Ilhan A. Aksay [b]

[a] Department of Advanced Nanostructured Materials Science and Technology, Kagoshima University, 1-21-40 Korimoto, Kagoshima 890-0065, Japan
[b] Department of Chemical Engineering, Princeton University, Engineering Quadrangle, Room A 311, Olden Street, Princeton, NJ, USA

Received 19 December 2008; received in revised form 21 February 2009; accepted 1 March 2009
Available online 27 March 2009

Abstract

This paper established a necessary condition for the sintering of powder compacts by examining the total free energy balance in terms of the particle size, neck size and contact number. The thermodynamic analysis of the proposed model clarifies the relation of shrinkage (q) of powder compact-contact angle (ϕ)-relative density at a given dihedral angle (ϕ_e) of a grain boundary. Faster densification proceeds in the region with a larger coordination number (n) of particles at a small q value. A large shrinkage is needed to eliminate the large pores formed in the structure of small n value. Full density can be achieved in the range of $117^\circ < \phi_e < \phi_c$, where ϕ_c is the critical dihedral angle allowing the shrinkage required for full densification. The derived concepts are effective to interpret the densification of hierarchical particle clusters. The relative density of ceria powder compact approached nonlinearly unity with decreasing ratio of pore size ($r(P)$) to grain size (r) and this tendency was well expressed by the present densification model. The influence of grain growth on the densification of powder compact and size of large pore isolated in a dense matrix are also quantitatively discussed.

Keywords: A. Sintering; B. Grain size; B. Porosity; D. CeO_2

1. Introduction

Sintering is the most fundamental process to densify a powder compact. During the sintering with shrinkage, the total solid volume is maintained to be a constant value but the shape and size of each particle change with the formation of grain boundaries. This change in solid particles is accompanied by the change of shape, size and fraction of pores in a unit volume [1]. The densification rate depends on the mass transport mechanisms [1]. The measured densification rate is referred to the proposed models to identify the dominant mass transport mechanism. In addition to the kinetic study of sintering, the microstructure evolution with densification is still important [1–4]. Our interest in sintering is to understand quantitatively the change of local microstructure with densification. An actual green compact includes the inhomogeneity of the packing of particles [1,5,6]. A green compact has a distribution of coordination number of particles at a given green density. Some particles are densely packed and some particles are loosely packed. When a powder compact is heated, the inhomogeneity of packing provides the different densification rates [1,5,7]. The whole microstructure represents the summation of the developed local microstructures. The understanding of the development of local microstructures with densification is the purpose of this paper. In this paper, the following relations are quantitatively analyzed: (1) dihedral angle-shrinkage of powder compact. This relation is influenced by coordination number of particles surrounding one particle. The model treated does not involve any sintering mechanisms but can be applied to actual solid state sintering. (2) Relative density of powder compact-contact angle between two particles during sintering. During the sintering a contact angle approaches the dihedral angle controlled by the ratio of grain boundary energy to surface energy. (3) Relative density-ratio of pore size to grain size. This proposed relation is compared with the sintering results of nanometer-sized ceria particles [8]. (4) Size of large pore coordinated by a large number of particles during sintering [1,2]. The derived relations explain well the previously reported microstructure evolution during sintering.

* Corresponding author. Tel.: +81 99 285 8325; fax: +81 99 257 4742.
E-mail address: hirata@apc.kagoshima-u.ac.jp (Y. Hirata).

0272-8842/$36.00
doi:10.1016/j.ceramint.2009.03.006

2. Sintering model

Fig. 1(a) shows the schematic model of sintering of spherical particles. Each particle of initial radius r_0 is surrounded by another n particles in a green compact. The sintering by heating forms the flat grain boundaries and the radius of particle changes to r. The overlapped solid volume V_1 in Fig. 1(b) is expressed by Eq. (1),

$$V_1 = \int_0^h \pi y^2 \, dx = \int_0^h \pi(r^2 - x^2) \, dx = \pi\left[r^2 h - \frac{h^3}{3}\right] \tag{1}$$

The remaining particle volume V_2 is expressed by Eq. (2),

$$V_2 = \frac{4}{3}\pi r^3 - nV_1 = \frac{4}{3}\pi r^3 - n\pi\left[r^2 h - \frac{h^3}{3}\right] \tag{2}$$

where n is the coordination number of particles. The ratio of h/r is written as p and Eq. (2) is expressed as a function of p.

$$V_2 = \pi r^3\left(\frac{4}{3} - np + \frac{np^3}{3}\right) \tag{3}$$

Since the volume of each particle is maintained as a constant value during the sintering, the following relation is derived.

$$\frac{4}{3}\pi r_0^3 = V_2 = \pi r^3\left(\frac{4}{3} - np + \frac{np^3}{3}\right) \tag{4}$$

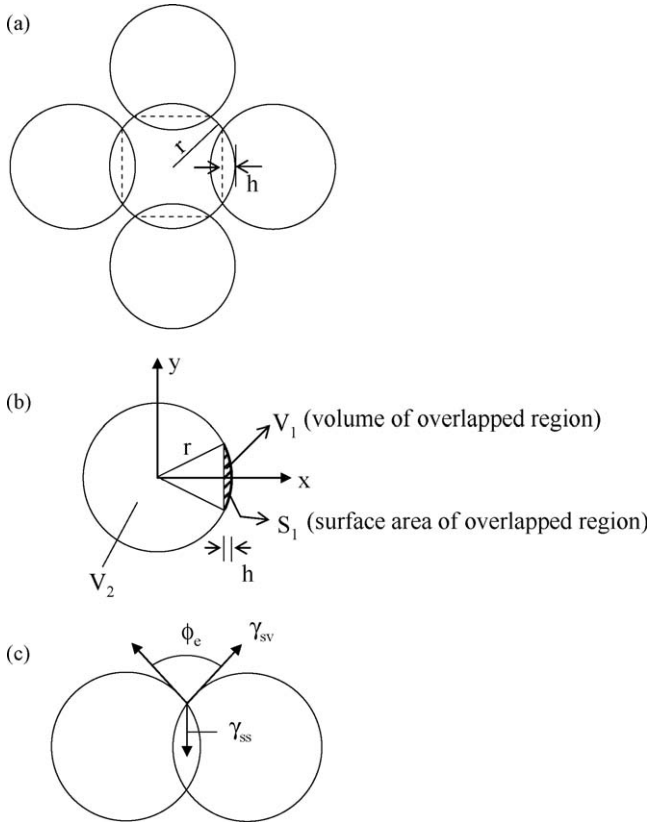

Fig. 1. Schematic model of sintering of spherical particle surrounded by another n particles (a). V_1 and S_1 in (b) represent the volume and surface area of overlapped region of thickness of h. (c) The dihedral angle (ϕ_e) under the equilibrium condition, which is related to the ratio of grain boundary energy (γ_{ss}) to surface energy (γ_{sv}) (Eq. (12)).

That is, r is expressed by Eq. (5),

$$r = r_0\left(\frac{4}{4 - 3np + np^3}\right)^{1/3} \tag{5}$$

The surface area (A_{sv}) corresponding to no overlapped region of one particle is given by Eq. (6),

$$A_{sv} = 4\pi r^2 - nS_1 \tag{6}$$

where S_1 is the surface area of over lapped region and can be calculated to be $2\pi rh$. The substitution of Eq. (5) for Eq. (6) results in Eq. (7).

$$\mathrm{Asv} = 4^{2/3}\pi r_0^2 \frac{4 - 2np}{(4 - 3np + np^3)^{2/3}} \tag{7}$$

On the other hand, the area of grain boundary (A_{ss}) is expressed by Eq. (8),

$$A_{ss} = \frac{n\pi}{2}\{r^2 - (r - h)^2\} = \frac{n\pi h}{2}(2r - h) = \frac{n\pi r^2}{2}(2p - p^2) \tag{8}$$

Since each solid–solid contact is shared by two particles, a factor 1/2 is put in front of Eq. (8). The driving force of sintering (Helmholtz energy, F) is given by Eq. (9),

$$dF = \gamma_{ss} dA_{ss} - \gamma_{sv} dA_{sv} \tag{9}$$

where γ_{ss} ($=\partial F/\partial A_{ss}$) and γ_{sv} ($=\partial F/\partial A_{sv}$) are the grain boundary energy and surface energy, respectively. From Eqs. (7) and (8), Eq. (9) is represented by Eq. (10) as a function of p,

$$\frac{1}{4^{2/3}\pi r_0^2}\frac{dF}{dp} = \gamma_{ss}\frac{n(1-p)[Z^{2/3} + np(1+p)(2-p)Z^{-1/3}]}{Z^{4/3}} + \gamma_{sv}\frac{2n[Z^{2/3} + (4-2np)(p^2-1)Z^{-1/3}]}{Z^{4/3}} \tag{10}$$

where Z is equal to $4 - 3np + np^3$. Densification proceeds under the condition of $dF/dp < 0$ and the condition of $dF/dp = 0$ indicates that the sintering process reaches an equilibrium. The necessary condition for sintering ($dF/dp \le 0$) leads to Eq. (11).

$$\frac{\gamma_{ss}}{\gamma_{sv}} \le -\frac{2[Z^{2/3} + (1-p^2)(2np-4)Z^{-1/3}]}{(1-p)[Z^{2/3} + np(1+p)(2-p)Z^{-1/3}]} \equiv T(p) \tag{11}$$

The right term in Eq. (11) is named $T(p)$ in this paper.

On the other hand, the dihedral angle ϕ_e (constant value) under the equilibrium condition (Fig. 1(c)) is related to the γ_{ss}/γ_{sv} ratio by Eq. (12).

$$\frac{\gamma_{ss}}{\gamma_{sv}} = 2\cos\left(\frac{\phi_e}{2}\right) \tag{12}$$

That is, densification proceeds under the following condition.

$$\cos\left(\frac{\phi_e}{2}\right) \le \frac{T(p)}{2} \tag{13}$$

The contact angle ($0 \leq \phi \leq \phi_e$) between two particles at an arbitrary p value approaches ϕ_e during the sintering.

3. Densification process

Fig. 2 shows the relationship between ϕ_e and p_e under the equilibrium condition for different coordination number of particles (Eq. (13)). Since V_2 value in Eq. (4) is a positive value, the condition of $Z \geq 0$ provides the minimum angle of ϕ_e, 117°, for n = 4–12. The ϕ_e value depends on the material used and is limited in the range of $117^\circ < \phi_e < 180^\circ$ in this model. As seen in Fig. 2, the p_e value (shrinkage expressed by h/r ratio) for a certain ϕ_e increases when n value decreases. When n is larger than 6, three-dimensional densification occurs. The structure of n = 6, 8 and 12 corresponds to simple cubic packing, body-centered cubic packing and cubic close packing, respectively. However, only one-dimensional densification occurs at n = 1 and 2 as seen Fig. 1(a). The condition of n = 3 represents two-dimensional densification and corresponds to the sintering of surface of powder compact. The condition of n = 4 provides both the possibilities of two-dimensional and three-dimensional densification, depending on the geometry of particle arrangement [4]. The decreased ϕ_e value allows the high shrinkage at a given coordination number of particles. Sinterability of particles may be controlled by the modification of surface characteristics of particle using sintering additives (control of γ_{sv} and γ_{ss} values).

Fig. 3 shows one example of the allowed sintering region of the particles with coordination numbers of n = 6–12 and dihedral angle (ϕ_e) of 117°. The ϕ_e value is independent of n value and depends only on the surface energy and grain boundary energy of particles. The starting point of sintering is $\phi = p = 0$. During the sintering, a powder compact shrinks with an increase in contact angle. The relation between shrinkage and contact angle depends on mass transport mechanisms and a simple linear relation is illustrated in Fig. 3 to understand the essence of densification. A larger shrinkage occurs for a smaller coordination number. The local microstructure with a different n value in a powder compact has a different contact angle at a given shrinkage. The relation between the densification (shrinkage) and contact angle is discussed in next section.

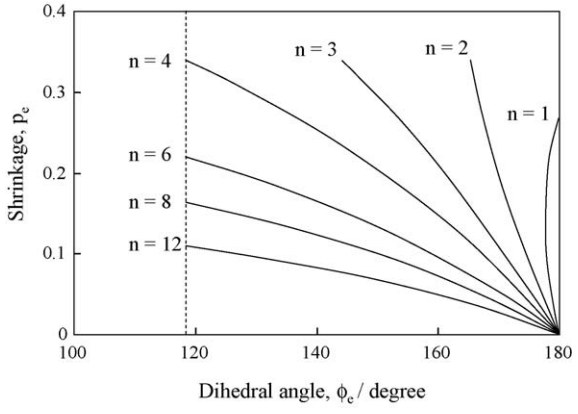

Fig. 2. Relation between ϕ_e and shrinkage p_e expressed by h/r ratio in Fig. 1(a) under the equilibrium condition (Eq. (11)).

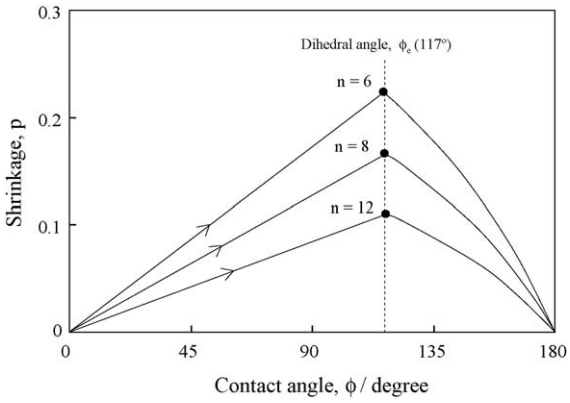

Fig. 3. One example of the allowed sintering region of particles with n = 6–12 and dihedral angle (ϕ_e) of 117°, shown as functions of contact angle between two particles and shrinkage (p).

4. Relation of shrinkage-relative density-contact angle

The solid fraction of sintered cubic compact with length of L (relative density, D) is expressed by Eq. (14),

$$L_0^3 D_0 = L^3 D \tag{14}$$

where L_0 and D_0 represent the length and packing density of green compact. The measurable shrinkage is expressed by Eq. (15),

$$\frac{L_0 - L}{L_0} = \frac{\Delta L}{L_0} = q \tag{15}$$

From Eqs. (14) and (15), D is expressed by Eq. (16) as a function of q.

$$D = \left(\frac{1}{1-q}\right)^3 D_0 \tag{16}$$

The pore volume in a sintered compact ($V(P)$) is also given by Eq. (17) using the relations by Eqs. (14) and (16),

$$V(P) = L^3(1-D) = \frac{D_0}{D} L_0^3 (1-D) = L_0^3[(1-q)^3 - D_0] \tag{17}$$

Fig. 4(a) shows Eq. (16) for D_0 = 0.524 (n = 6, simple cubic packing), 0.680 (n = 8, body-centered cubic packing) and 0.741 (n = 12, cubic close packing). The q value required for full densification is 0.194, 0.121 and 0.0953 for D_0 = 0.524, 0.680 and 0.741, respectively. Since only one q value is measured for one powder compact, the local microstructures with different n values have different relative densities. The close packing region reaches full density at q = 0.0953 but the other parts with smaller n values are porous. Further densification proceeds with an increase of q value in the region of n = 8. The mentioned relation in Fig. 4(a) produces the mixed microstructures of dense and porous regions at a given shrinkage. The distribution of local density in a sintered microstructure is affected by the inhomogeneity of starting powder compact. This concept is experimentally observed [1,5].

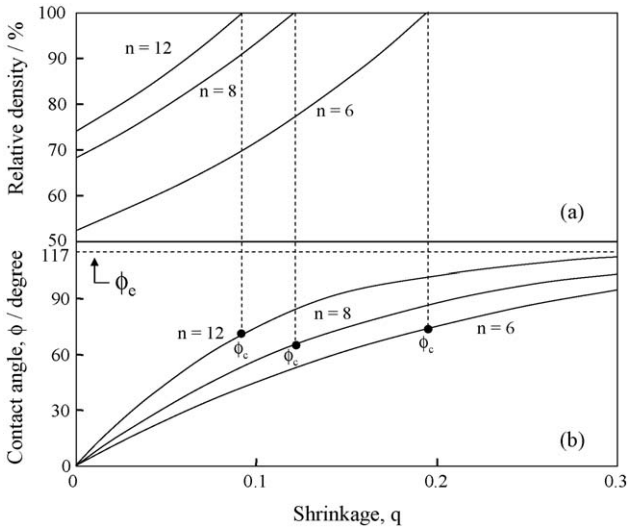

Fig. 4. (a) Relative density of powder compacts for $n = 6$–12 as a function of shrinkage (q) of powder compact ($q = (L_0 - L)/L_0 = h/r_0$, L_0: length of initial powder compact, r_0: initial particle size) (Eq. (16)). (b) The relation between contact angle (ϕ) and shrinkage (q) based on Fig. 3.

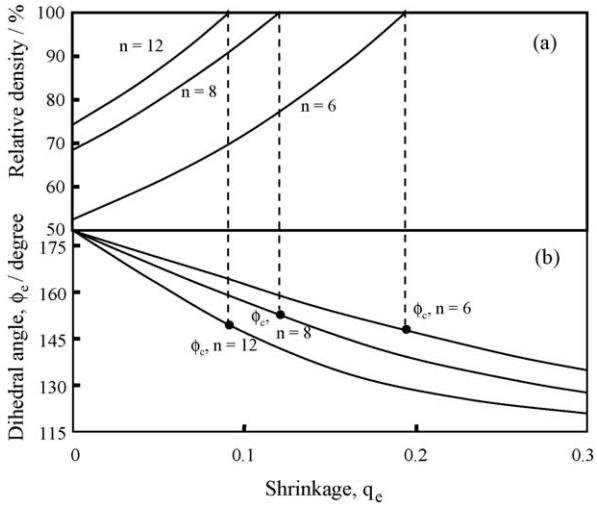

Fig. 5. (a) Relative density and shrinkage (q) under the equilibrium condition, which are controlled by the dihedral angle (b). Eqs. (11), (12) and (18) were used to construct (b).

Fig. 4(b) shows the relation between contact angle (ϕ) and q value. In Fig. 3, p value is defined by the ratio of h/r (Fig. 1(a)). On the other hand, q value is equal to the ratio of h/r_0 (r_0: initial particle radius). That is, q value is expressed by Eq. (18) using the relation of Eq. (5),

$$q = \frac{r}{r_0}p = \left[\frac{4}{4 - 3np + np^3}\right]^{1/3} p \tag{18}$$

The linear $p - \phi$ relation in Fig. 3 is changed to the nonlinear $q - \phi$ relation in Fig. 4(b). The contact angle ϕ becomes larger for a larger coordination number at a given shrinkage of q. In addition, it is understood that the local density for each n value reaches full density when ϕ_c for full density is smaller than ϕ_e. In Fig. 4(b), ϕ_e of 117° is given as a typical example. This relation is discussed more latterly. That is, the comparison of the results in Fig. 4(a) and (b) is summarized as follows: (1) faster densification at a small shrinkage proceeds in the region with a larger n value, (2) this densification is accompanied by the increase in contact angle, and (3) a porous local structure remains in the region with a small coordination number at a larger shrinkage.

Fig. 5(a) shows again the relative density as a function of q value (Eq. (16)) for $n = 6$, 8 and 12. Fig. 5(b) shows the relation between dihedral angle ϕ_e and corresponding final shrinkage q_e. This figure reflects the relation in Fig. 2 and is constructed using the relations of Eqs. (11) and (18). The final shrinkage q_e, which dominates the final relative density, is affected by dihedral angle ϕ_e. As seen in Fig. 5, the full densification is not achieved in the range of $180° > \phi_e > \phi_c$, where ϕ_c is the critical dihedral angle giving the shrinkage required for full densification. A large ϕ_e ($\phi_e > \phi_c$) results in a small shrinkage q_e, which determines the final low relative density of the local structure. On the other hand, it is possible to achieve the full density in the range of $\phi_c > \phi_e > 117°$. In this model ϕ_c is estimated to be 148–152° for $n = 6$–12. A small ϕ_e provides the large shrinkage (q_e) of sintering and the full density is achieved.

5. Pore size

During the sintering, the pore volume decreases as expressed by Eq. (17). The initial pore volume ($V(P_0)$) is $L_0^3(1 - D_0)$. The number of particles (N) in a green compact is $L_0^3 D_0/v$, where v represents the volume of one spherical particle of radius r_0 ($v = 4\pi r_0^3/3$). The pore volume belonging to each particle is given by Eq. (19),

$$v(P) = \frac{V(P)}{N} = \frac{L_0^3[(1-q)^3 - D_0]v}{L_0^3 D_0} = \frac{[(1-q)^3 - D_0]v}{D_0} \tag{19}$$

The radius of equivalent spherical pore ($r(P)$) for $v(P)$ is written as $v(P) = 4\pi r(P)^3/3$. That is, the size ratio of pore during the sintering to the initial pore is expressed by Eq. (20).

$$\frac{r(P)}{r(P_0)} = \left[\frac{(1-q)^3 - D_0}{1 - D_0}\right]^{1/3} \tag{20}$$

The $r(P_0)$ value for a green compact is equal to $r_0[(1 - D_0)/D_0]^{1/3}$ from Eq. (19), where r_0 is the radius of initial spherical particles. That is, the $r(P)/r_0$ ratio is expressed by Eq. (21),

$$\frac{r(P)}{r_0} = \left[\frac{(1-q)^3}{D_0} - 1\right]^{1/3} \tag{21}$$

On the other hand, $r(P)$ is usually compared with the grain size (r) during the sintering. The r/r_0 ratio is equal to q/p from Eq. (18). This relation is substituted for Eq. (21) to present $r(P)/r$ ratio (Eq. (22)).

$$\frac{r(P)}{r} = \frac{p}{q}\left[\frac{(1-q)^3}{D_0} - 1\right]^{1/3} \tag{22}$$

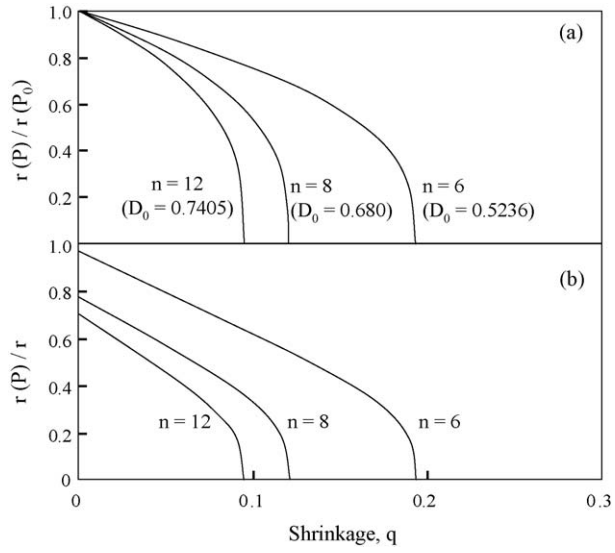

Fig. 6. (a) Size ratio of pore during sintering to the initial pore as a function of shrinkage q (Eq. (20)). (b) The size ratio of pore ($r(P)$) to grain (r) during sintering as a function of shrinkage, q (Eq. (22)).

Since q value is a function of p value (Eq. (18)), we can calculate Eq. (22) for an arbitrary q value. Fig. 6(a) and (b) shows the $r(P)/r(P_0)$ ratio (Eq. (20)), and $r(P)/r$ ratio (Eq. (22)), respectively. The pore size decreases gradually with increasing q value in the range of $1 > r(P)/r(P_0) > 0.3$. When the q value approaches the final q_e value for each coordination number of particles, the $r(P)/r(P_0)$ ratio drastically decreases. A similar tendency is observed in Fig. 6(b). The $r(P)/r$ ratio in the initial stage of q value decreases linearly with increasing q value. In the final stage of shrinkage, the $r(P)/r$ ratio is very sensitive to q value. At a certain q value, we observe a pore size distribution associated with the local structures of different relative densities depending on n values. The pores formed in the close packing structure disappear firstly at a given shrinkage. A larger shrinkage is needed to eliminate the pores formed in a packing structure of lower n value.

Fig. 7 shows the relationship between $r(P)/r$ ratio and relative density D calculated from Eqs. (16) and (22). This figure shows a similar densification tendency with $r(P)/r$ ratio for $n = 6$–12. Although the starting D_0 value is different, the local structure for each n value becomes denser at smaller $r(P)/r$ ratio. Especially, when the $r(P)/r$ ratio is less than 0.2, the relative density is close to full density. As discussed for the calculation in Fig. 6, the local structure for a larger n value provides a smaller $r(P)/r$ ratio at a given shrinkage, resulting in a high relative density. In a measured pore size distribution, the larger $r(P)/r$ ratio corresponds to the low density region for a small n value and the smaller pore size is related to the high density region for a large n value.

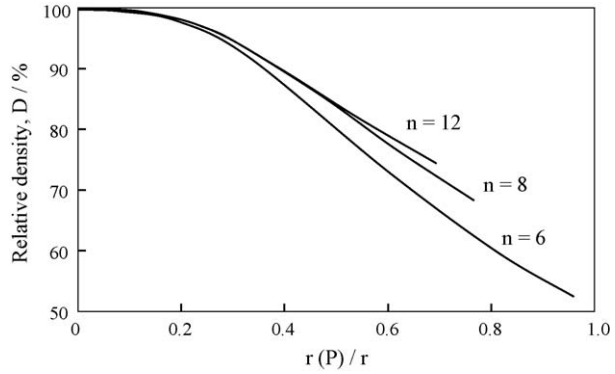

Fig. 7. Relation between relative density and $r(P)/r$ ratio for $n = 6$–12.

6. Shrink of large pore

We discuss the shrink of a large pore of radius $R(P_0)$ with the densification of a powder compact where a large amount of small pores of radius $r(P_0)$ are contained, as shown in Fig. 8(a). The change in size of small pores is discussed in Section 5. The densification of this powder compact is controlled by the faster shrink of small pores [1,5]. The shrink of small pores provides the influence on the local density and contact angle of particles surrounding the large pore (Fig. 8(b)). The large pore, which is surrounded by m particles (Fig. 8(b)), is treated as a curved plane of particle network of $n = 3$ (Fig. 8(c)). The ratio K_1 of cross sectional area of connected particles to the area of hexagonal unit cell is expressed by Eq. (23),

$$K_1 = \frac{[\pi r_0^2/3]6}{[r_0\sqrt{3}r_0/2]12} = \frac{\pi}{3\sqrt{3}} = 0.6046 \quad (23)$$

On the other hand, the ratio (K_2) of the cross sectional area of m particles to the surface area of large pore is approximated by

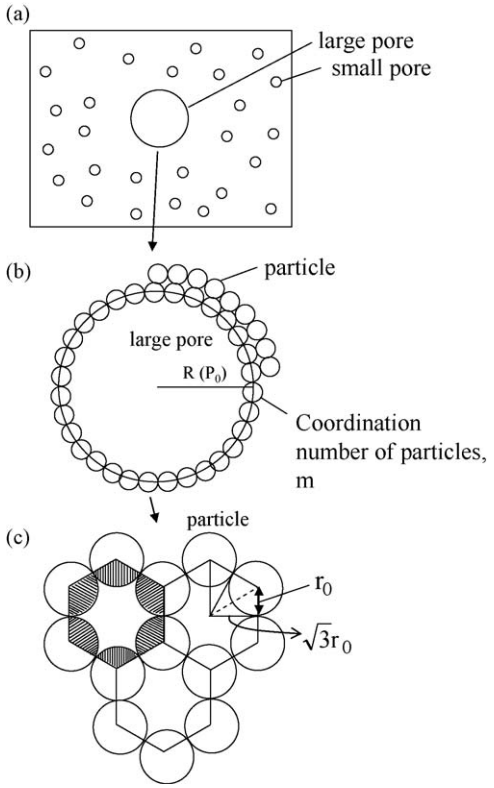

Fig. 8. (a) Schematic model of large pore coexisting with small pores. A large pore with radius $R(P_0)$ is surrounded by m particles with radius r_0 (b). The structure of m particles is treated as a curved plane of particles network of $n = 3$ (c).

Eq. (24),

$$K_2 = \frac{m\pi r_0^2}{4\pi R(P_0)^2} \tag{24}$$

Since K_1 in Eq. (23) is equal to K_2 in Eq. (24), the $R(P_0)/r_0$ ratio is given by Eq. (25).

$$\frac{R(P_0)}{r_0} = 0.643\sqrt{m} \tag{25}$$

The size of large pore is related to $m^{1/2}$. The shrinkage of powder compact (q) is dominated by the densification of particles associated with small pores (larger n values). The radius of large pore during the sintering is related to q by Eq. (26),

$$\frac{2\pi R(P_0) - 2\pi R(P)}{2\pi R(P_0)} = 1 - \frac{R(P)}{R(P_0)} = q \tag{26}$$

From Eqs. (25) and (26), the size of large pore during the sintering is expressed by Eq. (27).

$$\frac{R(P)}{r_0} = 0.643\sqrt{m}(1-q) \tag{27}$$

The q_e required full densification of particles with $n = 6$ and 12 is 0.0953 and 0.194, respectively. At q_e of shrinkage, the matrix is sintered to full density. Fig. 9 shows the $R(P)/r_0$ ratio for $q_e = 0.0953$ and 0.194 as a function of m value. When m value is in the range from 70 to 100, the large pore of $R(P)/r_0 \approx 5$ remains in the full density matrix. The larger pore of $R(P)/r_0 \approx 10$ is surrounded by fully sintered grains of 300–400. As seen in Fig. 9, the size of large pore isolated in the dense matrix is not sensitive to the n value of particles surrounding the small pore. In this model, the large pore is surrounded by particles of $n = 3$ (Fig. 8(c)). The two-dimensional packing density of surrounding particles is 0.605 (Eq. (23)). The shrinkage of for full densification of two-dimensional particles is calculated to be $q_e = 0.222$ because of the relations $L_0^2 D_0 = L^2 D$ and $1 - (L/L_0) = q$ (see Eqs. (14) and (15)). This shrinkage may limit the final size of large pore (Eq. (27)). Accurate experiment is needed to compare the proposed model.

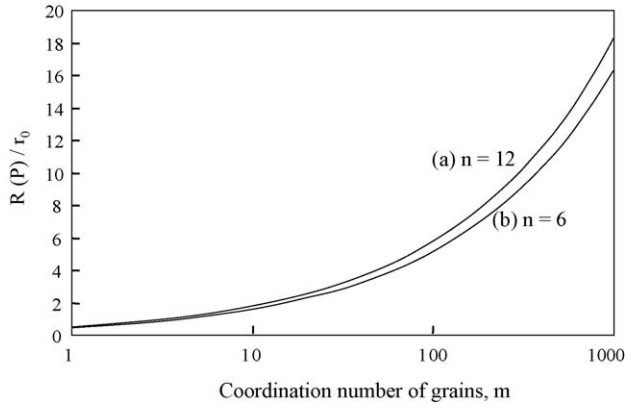

Fig. 9. Size ratio of large particle ($R(P)$) to initial particle size (r_0) when the small pores are eliminated completely from the matrix for $n = 6$ and 12, as a function of coordination number of grains surrounding the large pore.

7. Comparison of densification model and experimental results

We discussed the relationship of shrinkage-relative density-local microstructure (contact angle, dihedral angle, pore size) in Sections 2–6. The proposed model may be effective when the experimentally measured data are well interpreted by the model. Our group reported the sintering behavior of nanometer-sized ceria powder in a recent paper [8]. A part of the measured data is compared with the densification model shown in Fig. 7. The experimental procedure is briefly described. An aqueous suspension of 25 vol% ceria powder of 14 nm diameter (powder A) was consolidated by filtration through a gypsum mold. However, many cracks were formed during drying of ceria compact. Addition of large ceria powder of 37 nm diameter (powder B) to the 14 nm ceria powder was effective to prevent the formation of cracks. Therefore, the ceria powders of 14 and 37 nm diameters were mixed in an aqueous solution at pH 6 and consolidated by filtration though a gypsum mold. Some dried powder compacts were furthermore densified by cold isostatic pressing (CIP) at 196 MPa. The ceria green compacts were heated to 500–1600 °C at a rate of 10 °C min^{-1} and sintered for 1 h. The bulk density and apparent densities of sintered ceria were measured by the Archimedes method in distilled water. The microstructures of sintered ceria compact were observed by scanning electron microscope. The grain size of ceria in a sintered compact was measured by line intercept method on the polished and thermally etched surface of the ceria compact.

Fig. 10(a) shows the sintering behavior of the ceria compacts with 10 vol% powder B. The sintering behavior was characterized by the following four ranges: (I) first densification range at 500–800 °C, (II) first plateau of relative density at 800–1200 °C, (III) second densification range at 1200–1500 °C and (IV) second plateau of relative density at 1500–1600 °C. In

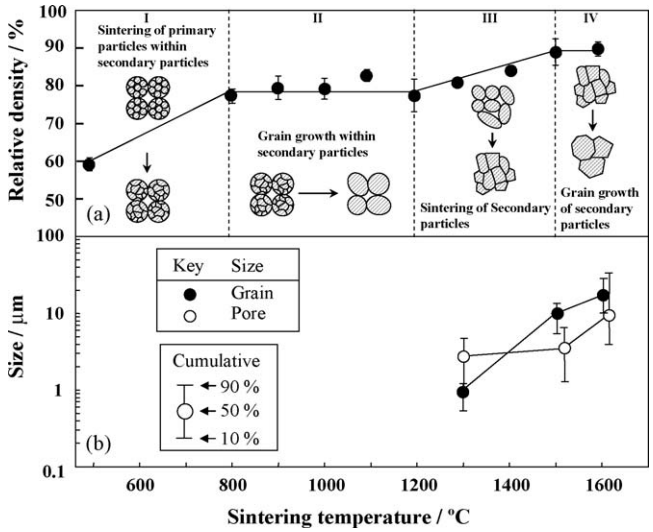

Fig. 10. (a) Relative density of ceria compact of mixed powders (90 vol% 14 nm particle −10 vol% 37 nm particles) as a function of sintering temperature for 1 h. (b) The pore size and grain size of ceria compacts sintered at 1300–1600 °C.

the range I, sintering of the nanometer-sized primary particles proceeds within secondary particle clusters [6,7]. The densification in the range I was characterized by the formation of closed pores at a lower relative density [8]. In the range II, little densification was measured and grain growth of secondary particles occurred. In the range III, pores are eliminated by the sintering of dense secondary grains after the grain growth of primary grains. The densification in the range III was seen with the formation of closed pores at a higher relative density [8]. In the range IV, grain growth of dense secondary particles proceeds drastically. In an actual sintering, alternative processes of densification and grain growth are observed with increasing sintering temperature. The densification model in this paper dose not deal with the grain growth but provides the interpretation for the measured result. Based on the calculated relation shown in Fig. 6, the small primary pores formed among densely packed primary particles are eliminated faster than the large secondary pores formed among secondary particles. The hierarchical sintering is related to the local densification shown in Figs. 4 and 6. On the other hand, the grain growth of the primary grains within a secondary particle cluster reduces the coordination number of grains surrounding a secondary pore. The ratio of size of secondary grain (R) after the grain growth to the diameter of primary particles (r_0) is written as $C(C = R/r_0)$. This relation is substituted for Eq. (27) to derive the $R(P)/R$ relation (Eq. (28)),

$$\frac{R(P)}{R} = 0.643\sqrt{\frac{m}{C^2}}(1-q) = 0.643\sqrt{m'}(1-q) \tag{28}$$

where m' is equal to m/C^2 and represents the coordination number of large secondary grains surrounding a secondary pore. The coordination number (m) of primary particles surrounding a large secondary pore decreases drastically to m/C^2 by grain growth. As a result, the $R(P)/R$ ratio results in a small value. When the $R(P)/R$ ratio becomes smaller than unity, the pore may be surrounded three-dimensionally by grains of $n = 6$–12 (Fig. 6). These pores are eliminated by the sintering of dense secondary grains. Therefore, the above grain growth in the range II provides the driving force (decrease of coordination number of grains to a pore) for the densification during the sintering [4]. The quantitative values of grain size and pore size are shown in Fig. 10(b) for the ceria compact with 10 vol% powder B. The pore size was almost constant in the range III (1300–1500 °C) and increased in the range IV (1500–1600 °C). On the other hand, the grain size of ceria increased continuously in the range III and IV [1,6]. These changes in the grain size and pore size effectively reduced the ratio of pore size to grain size with increasing temperature. That is, the coordination number of ceria grains to a pore decreased at a higher sintering temperature in the range III.

Fig. 11 summarizes the relationship between the ratio of pore size to grain size and relative density of powder compact with 10–60 vol% powder B in the ranges III and IV. In Fig. 11, the $r(P)/r$ ratio-relative density relation shown in Fig. 7 is also plotted to interpret the measured data. It is apparent that the densification is enhanced as the ratio of pore size to grain size decreased. The

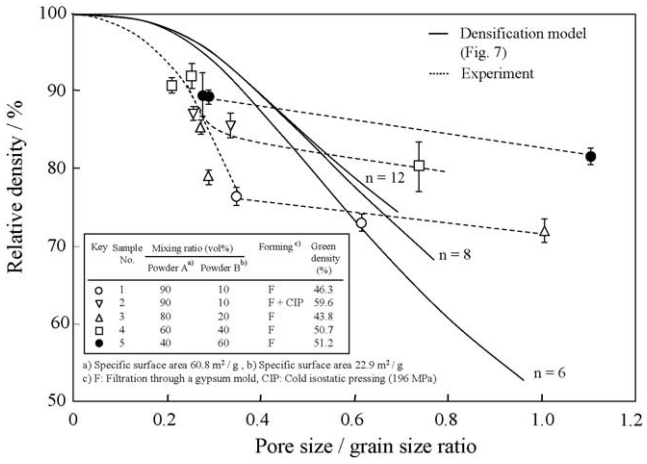

Fig. 11. Relationship between the ratio of pore size ($r(P)$) to grain size (r) and relative density of powder compacts with 10–60 vol% 37 nm particles. In figure, the $r(P)/r$ ratio-relative density relation for the densification model shown in Fig. 7 is also plotted to compare with the measured relation.

measured tendency agreed with the prediction from the present model. The difference of relative density between the experiment and model may be related to the wider size distributions of grains and pores in the actual powder compacts.

8. Conclusions

A densification model of particle coordinated by n particles was analyzed using the Helmholtz energy represented by the summation of surface energy of particles and grain boundary energy. The derived important concepts are follows. The dihedral angle (ϕ_e) at the grain boundary, which is related to the ratio of grain boundary energy to surface energy, is limited in the range of $117^\circ < \phi_e < 180^\circ$ in the present model. The decreased ϕ_e value allows a large shrinkage (q) at a given coordination number (n) of particles. A large shrinkage occurs for a smaller n value. Faster densification at a small shrinkage proceeds in the region with a large n value. This densification is accompanied by the increase in contact angle (ϕ). A porous local structure remains in the region with a small n value at a given shrinkage. It is possible to achieve full density in the range of $117^\circ < \phi_e < \phi_c$, where ϕ_c is the critical dihedral angle giving the shrinkage required for full density. When the shrinkage (q) approaches the final q_e value for each n value, the ratio of pore size ($r(P)$) to initial pore size ($r(P_0)$), $r(P)/r(P_0)$, results in 0. The pores formed in the close packing structure disappear firstly at a given shrinkage. A larger shrinkage is needed to eliminate the large pores formed in the structure of smaller n value. Similarly, the small primary pores formed among densely packed primary particles are eliminated faster than the large secondary pores formed among secondary particle clusters. The grain growth of primary grains within a secondary particle cluster reduces the coordination number of grains surrounding a secondary pore, enhancing the driving force for densification. The measured relative density increased nonlinearly with decreasing $r(P)/r$ (grain size) ratio and this tendency was well explained by the present model. The size of large pore isolated in the dense matrix is related to the

coordination number (m) of primary particles surrounding the large pore and shrinkage of matrix. The coordination number decreases drastically to m/C^2, where C is the ratio of size (R) of grain after grain growth to the diameter (r_0) of primary particle.

References

[1] W.D. Kingery, H.K. Bowen, D.R. Uhlmann, Introduction to Ceramics, John Wiley Sons Inc., New York, 1976, pp. 448–515.
[2] B.J. Kellett, F.F. Lange, Thermodynamics of densification: sintering of simple particle arrays, equilibrium configurations, pore stability and shrinkage, J. Am. Ceram. Soc. 72 (5) (1989) 725–734.
[3] F.F. Lange, B.J. Kellett, Thermodynamics of densification: II, grain growth in porous compacts and relation to densification, J. Am. Ceram. Soc. 72 (5) (1989) 735–741.
[4] F. Wakai, Modeling and simulation of elementary processes in ideal sintering, J. Am. Ceram. Soc. 89 (5) (2006) 1471–1484.
[5] F.F. Lange, Sinterability of agglomerated powders, J. Am. Ceram. Soc. 67 (2) (1984) 8389.
[6] Y. Hirata, I.A. Aksay, R. Kikuchi, Quantitative analysis of hierarchical pores in powder compact, J. Ceram. Soc. Jpn. 98 (2) (1990) 126–135.
[7] M.D. Sacks, J.A. Pask, Sintering of mullite-containing materials: II, effect of agglomeration, J. Am. Ceram. Soc. 65 (2) (1982) 70–77.
[8] Y. Hirata, A. Harada, X.H. Wang, Wet forming and sintering behavior of nanometersized ceria powder, Ceram. Inter. 31 (2005) 1007–1013.